Wide-slit diffraction and wavefront diagnostics of optical-vortex beams

Bekshaev A. Ya., Kurka I. A., Mohammed K. A. and Slobodeniuk I. I.

I. I. Mechnikov Odesa National University, 2 Dvorianska Street, 65082 Odesa, Ukraine, bekshaev@onu.edu.ua

Abstract. A slit diffraction is widely used for express diagnostics of optical vortices (OVs). We propose a version of this method that employs relatively wide slits of the sizes comparable with the thickness of bright ring characterizing the OV-beam under test. Under such conditions the diffracted beam contains two bright lobes that propagate along the directions determined by local normals to the incident-beam wavefront in the slit plane. As a result, observations of the lobes' displacements within the beam cross section provide information on the local wavefront slope and, consequently, on the OV sign and topological charge. The evolution of the lobes' positions during the diffracted beam propagation visualizes a hidden energy circulation in the incident OV-beam and provides a direct and spectacular illustration of the internal energy flows.

1. Introduction

Light beams bearing optical vortices (OVs) [1–4] are very interesting objects with rich physical meaning, which has inspired far-reaching reminiscence and analogies from the whole physical world. Their essential property is presence of a circulatory energy flow (a transverse energy circulation effect abbreviated hereafter as TEC) that accompanies longitudinal energy transportation usual for light fields. The TEC is coupled with another characteristic feature, a phase singularity, which manifests itself as a spatial point with zero field amplitude, in the vicinity of which the beam wavefront possesses a screw-like shape. These features are associated with accompanying mechanical properties, especially a nonzero orbital angular momentum of the beam with respect to the propagation axis. The unique OV properties have been employed in many applications, e.g. in micromanipulation techniques or information processing [5, 6]. However, maybe, a more important fact is that a specific pattern of the energy flow in the OVs makes them suitable model objects while studying the internal energy flows in the light fields [7].

Most immediately, specific physical properties of the OVs can be observed in the effects that accompany OV-beam propagation in the presence of some obstacles, in particular, the diffractions at an edge [8–16], a slit [11, 15], or a strip [16, 17]. These effects are employed in numerous applications aimed at detecting and diagnosing the OVs [16–19], as well as in the sub-wavelength optical metrology [20, 21]. The matter is that a peculiar pattern of the internal energy flows, usually hidden in the OV-beams with circularly-symmetric structures, becomes immediately visible due to the diffraction processes and can thus be efficiently detected and measured. There are a number of ingenious propositions on how the diffraction patterns can be utilized for the OV-

beams diagnostic and characterization [15–19]. In this article, we describe a version of a slit-diffraction approach whose distinctive feature is immediate appeal to the internal energy circulation, which represents its physical background in an impressive and transparent form.

2. Experiment

We use a traditional scheme for obtaining the OV-beams [2, 3, 22]. Omitting details of the routine, the OV is generated by transmitting a Gaussian beam produced by a He-Ne laser (the wavelength $\lambda = 0.6328 \ \mu m$) through a 'fork' hologram with its central groove split into three branches. Such a hologram produces a series of diffracted beams carrying OVs with the topological charges $m = \pm 2, \pm 4, \pm 6, \dots$ [22]. To be specific, below we describe the results obtained with the first- and second-order diffracted beams carrying circularly symmetric OVs with $m = 2$ and $m = 4$.

After spatial isolation of a chosen beam, it is directed onto a non-transparent screen with a vertical slit-like outlet. The intensity profiles for the selected beams in the screen plane are presented in Fig. 1a. As usual, they contain axial amplitude zeros and bright rings which, in our situation, have the diameters $d = 1.5$ mm (for $m = 2$) and $d = 1.8$ mm (for $m = 4$). In contrast to the usual slit-diffraction schemes [17], the slit width is comparable with the width of the bright ring of the OV-beams and amounts to 0.5 mm (see Fig. 1b). The beams and the slit are adjusted so as the central line of the slit crosses the beam axis; the beam axis is identified with the axis z of the laboratory coordinate system.
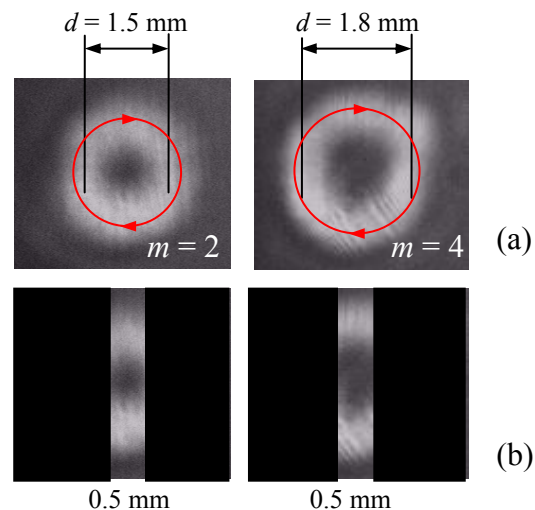

Fig. 1. (a) Transverse intensity profiles of OV-beams, as seen along the beam propagation direction: arrows show TEC directions for the positive OVs (diameters of the bright rings and topological charges of the OVs are indicated); (b) Beam patterns observed immediately behind the screen, with slit width indicated.

The beams freely propagate after passing the screen, and the diffraction patterns are detected at several distances $z = z_i$ from the screen by means of a CCD camera (the sensing area 4×3 mm^2 and the resolution 704×576 pixels) and analyzed with a PC. The corresponding intensity distributions are illustrated in Fig. 2.

The images presented show usual diffraction fringes. Their shapes and orientations can serve while detecting the sign and the strength of the incident OV [17–19]. Since now the fringes are not of our main interest, instead we focus on a visible evolution of the two main intensity maxima formed after the slit (see Fig. 1b). One can easily see from Fig. 2 that transformation of the two-

lobe pattern distinctly 'brings to light' the TEC of the incident OV-beam (cf. Fig. 1a). In full agreement with the internal energy circulation, the upper lobe moves to the right and the lower one to the left, thus performing a circulatory motion in accordance with the 'initial' transverse momentum 'acquired' by the lobes from the TEC of the incident beam. Simultaneously, vertical displacements of the lobes are seen which reflect an off-centre energy spreading due to the beam divergence.

$z = z_1 = 52.4$ cm $\qquad\qquad z = z_2 = 86.0$ cm $\qquad\qquad z = z_3 = 135.4$ cm
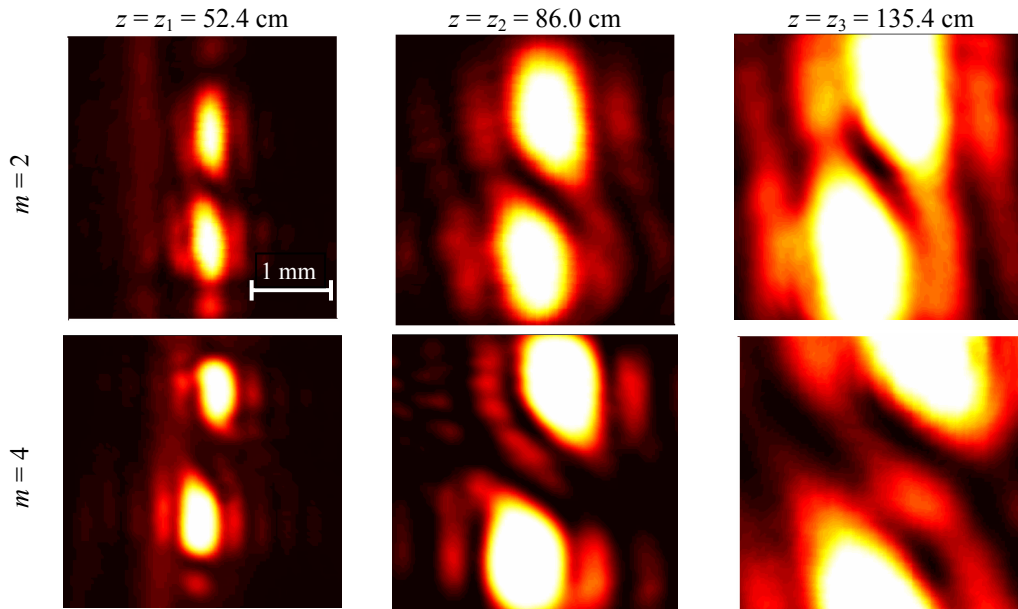
Fig. 2. Slit-diffraction patterns observed for different distances behind the screen, which are marked above each column. The first and second rows of the images correspond to OV-beams with the topological charges $m = 2$ and $m = 4$, respectively.

To attribute a quantitative sense to these qualitative observations, we consider more thoroughly the characteristics of the beam-spot patterns for different distances z_i in a single plot. Fig. 3 represents the behaviour of the diffracted beam with a 2-charged OV (this corresponds to the first row of images in Fig. 2). Current positions of the upper and lower bright lobes seen in Fig. 2 are characterized by the centre of gravity (CG) coordinates defined as

$$\begin{pmatrix} x_{Ci}^+ \\ y_{Ci}^+ \end{pmatrix} = \frac{\int_{-\infty}^{+\infty} dx \int_0^\infty dy \begin{pmatrix} x \\ y \end{pmatrix} I(x,y,z_i)}{\int_{-\infty}^{+\infty} dx \int_0^\infty dy I(x,y,z_i)} , \begin{pmatrix} x_{Ci}^- \\ y_{Ci}^- \end{pmatrix} = \frac{\int_{-\infty}^{+\infty} dx \int_{-\infty}^0 dy \begin{pmatrix} x \\ y \end{pmatrix} I(x,y,z_i)}{\int_{-\infty}^{+\infty} dx \int_{-\infty}^0 dy I(x,y,z_i)} , \qquad (1)$$

with $I(x,y,z_i)$ being the transverse intensity distribution measured in the cross section $z = z_i$ ($i = 1, 2, 3$). Fig. 3 demonstrates, in a spectacular manner, how the beam energy is redistributed during the free propagation. Here the displacements of the CG (denoted with black asterisks) agree with a qualitatively visible overall energy motion (see arrows). In further consideration, we discard the vertical displacements associated with a usual beam divergence and concentrate on the horizontal components which are more important for OV diagnostics, because these components immediately testify for a TEC present in the incident OV-beam.
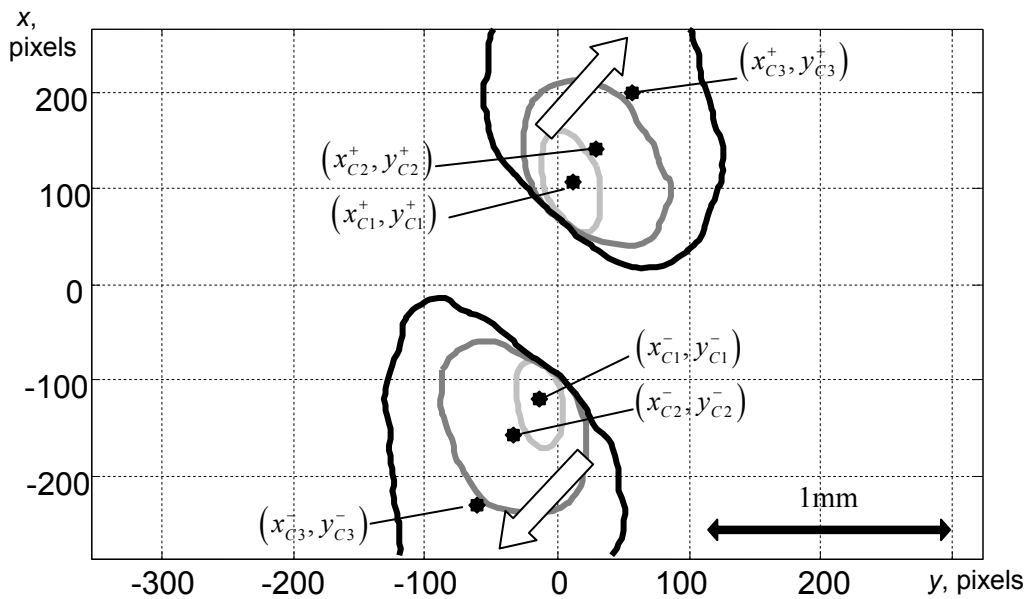
Fig. 3. Constant-intensity contours (75% of maximum) for diffracted-beam images displayed in the first row of Fig. 1 ($m = 2$): $z = z_1$ (light grey), $z = z_2$ (grey), and $z = z_3$ (black). Black asterisks denote CG positions for the upper (+) and lower (−) bright lobes given by Eqs. (1), and arrows show overall directions of the transverse energy motion. Point (0, 0) belongs to axis z of the incident beam.

To decrease the harmful influence of random illumination noise and possible inaccuracies in recording the beam axis, it would be suitable to characterize the horizontal CG displacements by the relevant mean values:

$$x_{Ci} = \frac{x_{Ci}^+ - x_{Ci}^-}{2} . \tag{2}$$

The results are collected in Table 1 and Fig. 4. A similar analysis has been performed for the beam with the 4-charged OV (see second row of images in Fig. 2). The corresponding data are also presented in Table 1 and Fig. 4.

Table 1. CG positions of the lobes for propagating diffracted beams, and derivation of wavefront parameters of the incident-beam.

Parameters of the incident OV (see Fig. 1)	x_{C1}, mm	x_{C2}, mm	x_{C3}, mm	Angle between the CG trajectory and the axis z of the incident beam (mean x_{Ci}/z_i), mrad	Angle of the wavefront slope α (see Eq.(3)), mrad
$m = 2$, $d = 1.5$ mm	0.08	0.22	0.37	0.253	0.267
$m = 4$, $d = 1.8$ mm	0.20	0.43	0.72	0.490	0.446

The data displayed in Fig. 4 shows that the transverse displacements of the lobes increase linearly with increasing propagation distance, i.e. the CG trajectory for each lobe is a straight line. This agrees with the known geometric features of the CG trajectories for a free-propagating beam [23] and supports the idea that the separate lobes of the diffracted beams propagate almost independently. For the beam with the higher-order OV ($m = 4$), the displacements are, on the

average, twice larger than those peculiar for the lower-order one ($m = 2$), which is quite expected because of the higher OV strength. Such behaviour can be interpreted in view of the fact that in scalar beams, the light energy propagates along the wavefront normals [7]. Actually, the slit 'cuts' a certain area within the incident-beam cross section, and the transmitted energy 'contained' within this area propagates along the local wavefront normal. Therefore, the angular deviation of the lobe's trajectory determined as a mean value of the ratio x_{Ci}/z_i (see the fifth column in Table 1) can be a measure of local azimuthal slope of the incident-beam wavefront.
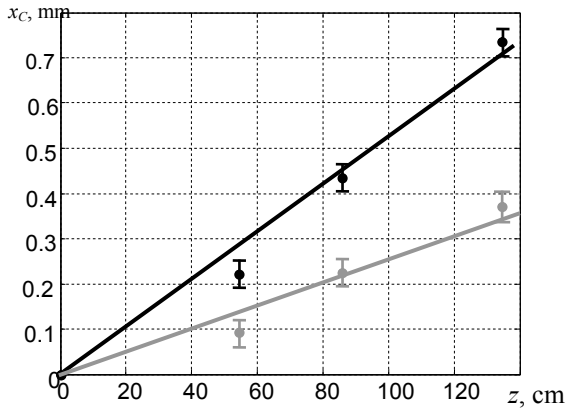

Fig. 4. Horizontal displacements of lobes of the diffracted beam as functions of the propagation distance behind the screen, as calculated with the images of Fig. 2 (data points), and their linear fits (lines). Grey and black colours correspond to the incident OV-beams with $m = 2$ and $m = 4$, respectively.

Based on a helical wavefront shape for circularly symmetric OVs (see Fig. 5), one can compare this result with what is expected from the usual OV model. On round-tripping near the m-charged OV core, the phase increment is equal to $m\lambda$ [1–3] and the round-trip length along the bright ring amounts to πd (see Fig. 1a). Then the azimuthal wavefront slope is given by

$$\alpha = \frac{m\lambda}{\pi d} \,. \tag{3}$$

The corresponding values of the angle α obtained for the OV-beams under consideration are presented in the sixth column of Table 1. Their accordance with the measured angular deviations of the diffracted-beam lobes (see the fifth column of Table 1) looks quite satisfactory, especially in view of a simplicity of experimental technique employed and a non-ideal OV structure of the incident beam (cf. Fig. 1a).
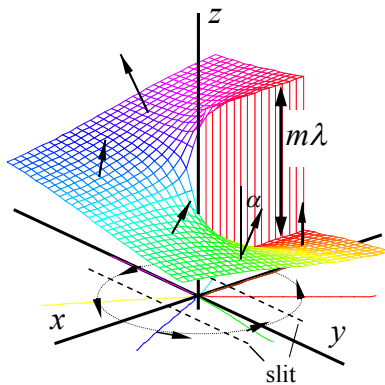
Fig. 5. Wavefront of an OV-beam near OV-core. Normals to a screw-like surface make an angle α with respect to longitudinal direction, while their azimuthal components form a close-loop circulation in the beam cross section. Traces of the slit edges are shown by dashed lines.

3. Conclusions

In this work we have described a new approach to diagnosing the wavefronts of OV-beams, which is based on the slit-diffraction. Unlike the earlier diffraction techniques, the procedure suggested here involves observations of the diffracted beam evolution rather than the diffraction-fringe shape and bending. In fact, our method may be considered as an extremely simplified version of a known Shack–Hartmann method for wavefront sensing [7, 24] where the beam transverse section is fractionated into a number of 'beamlets' that propagate independently in the directions determined by the local wavefront normals. In the present case, the two 'beamlets' are formed by joint action of the slit and a ring-like structure of the incident beam, which makes the method remarkably simple and easy-to-implement.

In its present form, our method is rather specialized, being adapted predominantly to circularly symmetric OV-beams. However, when supplemented with the means for real-time beam positioning and orienting, it can be generalized and applied to more complicated OV-beams, e.g. anisotropic and deformed ones. Nevertheless, even in its simplest version, our method proves to be useful for approximate express diagnostics of the usual OV-beams. Moreover, it can be helpful in the practice of physical education since provides demonstration of the internal energy flow and its vortex character in a rather immediate and impressive manner.

References

1. Allen L, Padgett M J and Babiker M, 1999. Orbital angular momentum of light. Prog. Opt. **39**: 291–372.
2. Soskin M S and Vasnetsov M V, 2001. Singular optics. Prog. Opt. **42**: 219–276.
3. Bekshaev A Ya, Soskin M S and Vasnetsov M V. Paraxial light beams with angular momentum. N. Y.: Nova Science Publishers, 2008.
4. Dennis M R, O'Holleran K and Padgett M J, 2009. Singular optics: optical vortices and polarization singularities. Prog. Opt. **53**: 293–363.
5. Dienerowitz M, Mazilu M and Dholakia K, 2008. Optical manipulation of nanoparticles: a review. J. Nanophotonics. **2**: 021875.
6. Bowman R W and Padgett M J, 2013. Optical trapping and binding. Rep. Prog. Phys. **76**: 026401.
7. Bekshaev A, Bliokh K and Soskin M, 2011. Internal flows and energy circulation in light beams. J. Opt. **13**: 053001.
8. Vasnetsov M V, Marienko I G and Soskin M S, 2000. Self-reconstruction of an optical vortex. JETP Lett. **71**: 130–133.
9. Gorshkov V N, Kononenko A N and Soskin M S, 2001. Diffraction and self-restoration of a severe screened vortex beam. Proc. SPIE. **4403**: 127–137.
10. Gorshkov V N, Khoroshun A N and Soskin M S, 2006. Diffraction of the singular beam on an opaque screen and regeneration of an optical vortex. Ukr. J. Phys. **51**: 132–139.
11. Masajada J, 2000. Gaussian beams with optical vortex of charge 2- and 3-diffraction by a half-plane and slit. Opt. Applicata. **30**: 248–256.
12. Masajada J, 2000. Half-plane diffraction in the case of Gaussian beams containing an optical vortex. Opt. Commun. **175**: 289–294.
13. Pusheng Liu and Baida Lü, 2008. Propagation of Gaussian background vortex beams diffracted at a half-plane screen. Opt. Laser Technol. **40**: 227–234.

14. Yamei Luo, Zenghui Gao, Bihua Tang and Baida Lü, 2013. Electric and magnetic polarization singularities of first-order Laguerre-Gaussian Beams diffracted at a half-plane screen. J. Opt. Soc. Amer. A. **30**: 1646–1653.

15. Arlt J, 2003. Handedness and azimuthal energy flow of optical vortex beams. J. Mod. Opt. **50**: 1573–1580.

16. Cui H X, Wang X L, Gu B, Li Y N, Chen J and Wang H T, 2012. Angular diffraction of an optical vortex induced by the Gouy phase. J. Opt. **14**: 055707.

17. Devinder Pal Ghai, Senthilkumaran P and Sirohi R S, 2009. Single-slit diffraction of an optical beam with phase singularity. Opt. Lasers Eng. **47**: 123–126.

18. Bogatyryova H V, Felde Ch V and Polyanskii P V, 2003. Referenceless testing of vortex optical beams. Opt. Applicata. **33**: 695–708.

19. Felde Ch V, 2004. Diffraction diagnostics of phase singularities in optical fields. Proc. SPIE. **5477**: 67–76.

20. Masajada J, Leniec M, Drobczyński S, Thienpont H and Kress B, 2009. Micro-step localization using double charge optical vortex interferometer. Opt. Express. **17**: 16144–16159.

21. Masajada J, Leniec M, Jankowska E, Thienpont H, Ottevaere H and Gomez V, 2008. Deep microstructure topography characterization with optical vortex interferometer. Opt. Express. **16**: 19179–19191.

22. Bekshaev A Ya, Bekshaev A S and Mohammed K A, 2014. Arrays of optical vortices formed by 'fork' holograms. Ukr. J. Phys. Opt. **15**: 123–131.

23. Marcuse D. Light Transmission Optics. N. Y.: Van Nostrand Reinhold, 1982.

24. Optical Shop Testing. Ed. D. Malacara. Hoboken, N. J.: Wiley-Interscience, 2007.

Анотація. Дифракцію на щілині широко застосовують для експрес-діагностики оптичних вихорів (ОВ). Ми пропонуємо варіант цього методу, який використовує досить широку щілину з розміром, близьким до ширини світлого кільця досліджуваного ОВ-пучка. За цих умов дифрагований пучок містить два яскраві максимуми, що поширюються в напрямках, визначених локальними нормалями до хвильового фронту падаючого пучка в площині екрану. Їх спостереження надає інформацію про локальний нахил фронту, а отже, про знак і топологічний заряд ОВ. Еволюція розташування максимумів у процесі поширення дифрагованого пучка дає змогу візуалізувати поперечну циркуляцію енергії, яка приховано відбувається в падаючому ОВ-пучку, і може слугувати безпосередньою і наочною ілюстрацією внутрішніх потоків енергії.